JACS
JOURNAL OF THE AMERICAN CHEMICAL SOCIETY
Article
pubs.acs.org/JACS

Modulation of Thermoelectric Power Factor via Radial Dopant Inhomogeneity in B-Doped Si Nanowires

Fuwei Zhuge,[†] Takeshi Yanagida,*[,†] Naoki Fukata,[‡] Ken Uchida,[§] Masaki Kanai,[†] Kazuki Nagashima,[†] Gang Meng,[†] Yong He,[†] Sakon Rahong,[†] Xiaomin Li,[∥] and Tomoji Kawai[†]

[†]Institute of Scientific and Industrial Research, Osaka University, 8-1 Mihogaoka, Ibaraki, Osaka 567-0047, Japan
[‡]National Institute for Material Science, 1-1 Namiki, Tsukuba, Ibaraki 305-0044, Japan
[§]Department of Electrical Engineering, Keio University, 3-14-1 Hiyoshi Kouhokuku Yokohama 223-8522, Japan
[∥]Shanghai Institute of Ceramics, Chinese Academy of Sciences, Shanghai 200050, China

Supporting Information

ABSTRACT: We demonstrate a modulation of thermoelectric power factor via a radial dopant inhomogeneity in B-doped Si nanowires. These nanowires grown via vapor−liquid−solid (VLS) method were naturally composed of a heavily doped outer shell layer and a lightly doped inner core. The thermopower measurements for a single nanowire demonstrated that the power factor values were higher than those of homogeneously B-doped Si nanowires. The field effect measurements revealed the enhancement of hole mobility for these VLS grown B-doped Si nanowires due to the modulation doping effect. This mobility enhancement increases overall electrical conductivity of nanowires without decreasing the Seebeck coefficient value, resulting in the increase of thermoelectric power factor. In addition, we found that tailoring the surface dopant distribution by introducing surface δ-doping can further increase the power factor value. Thus, intentionally tailoring radial dopant inhomogeneity promises a way to modulate the thermoelectric power factor of semiconductor nanowires.

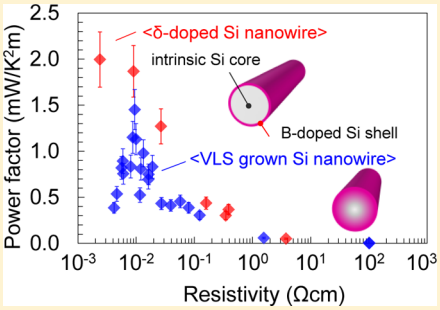

1. INTRODUCTION

Thermoelectric power generation holds great promise for waste heat recovery.[1] Intensive efforts have been devoted to improve the energy conversion efficiency of thermoelectric devices.[2−4] The figure of merit ZT is well-known to determine the conversion efficiency, which is defined as $S^2T/\rho\kappa$, where S, ρ, κ, and T are the Seebeck coefficient, electrical resistivity, thermal conductivity, and temperature, respectively. However, due to the strong intercorrelation between these parameters,[4] enhancing the ZT value has been limited in bulk materials. Decreasing the thermal conductivity via increasing the phonon scattering in nanostructures has been a promising approach to improve the ZT.[2−4] Among various nanostructures, self-assembled semiconductor nanowires hold great promise for improving the ZT. For example, Hochbaum et al.[5] and Boukai et al.[6] have reported the significant enhancement of ZT in chemically etched Si nanowires, which have been interpreted in terms of the decreased thermal conductivity. Another possible advantage of nanowires is the potential to increase the thermoelectric power factor by decoupling S and ρ via low dimensional effect.[7] Recently, Tian et al.[8] and Wu et al.[9] have observed the enhancement of Seebeck coefficient values due to the low dimensional quantum effect using InAs nanowires. However, such quantum effects have been observed only at low temperature range below 100 K due to perturbations from surroundings.[8] Although the thermal conductivity has been successfully reduced for various nanowires, maintaining and/or increasing the power factor (S^2/ρ) of nanowires at room temperature has been difficult due to the surface states, which reduces the mobility and conductivity via the surface trapping and scattering.[10,11] One simple solution to overcome this issue is to create the mobile carriers far from the nanowire surface. Utilizing a core/shell structure might be the solution to achieve this.[12−15] Moon et al. have demonstrated that the power factor of Ge/Si core/shell nanowires exceeded that of bulk value.[15] The hole trasnport of Ge nanowire confined by energy band offset allowed an enhancement of hole mobility.[15] Although intentionally controlling the radial dopant inhomogeneity might be a promising way to create such high mobility carriers even without the use of heterointerfaces,[16] the role of radial dopant inhomogeneity on thermoelectric power factor of nanowires has not been clarified yet. The spatial dopant distributions at the nanoscale in semiconductor nanowires have been an important issue to control the transport properties.[17−21] It has been shown that a dopant inhomogeneity exists along the radial direction for vapor−liquid−solid (VLS) grown Si and Ge nanowires.[21] For example, B doping in VLS grown Si nanowires has resulted in a heavily doped outer shell layer and a lightly doped core due to the naturally occurring sidewall vapor−solid (VS) growth.[17] Since the inhomogeneous dopant spatial distribution is highly detrimental for the applications to

Received: June 3, 2014
Published: September 17, 2014

dx.doi.org/10.1021/ja5055884 | J. Am. Chem. Soc. 2014, 136, 14100−14106

electrical devices of nanowires, intensive efforts have been carried out to achieve uniform dopant distribution.[21,22] In this study, we aim to utilize the previously detrimental dopant spatial inhomogeneity to modulate the thermoelectric power factor of Si nanowires.

2. EXPERIMENT AND METHODS

2.1. Growth of Si Nanowires. B-doped Si nanowires were grown by Au catalyzed VLS process using a chemical vapor deposition (CVD) system. Si(111) wafer was used as the substrate. The growth time was ~30 min. The growth temperature was set to be 600 °C, and then the vapor sources of SiH_4 (19 sccm) and B_2H_6 (0.2 sccm) were introduced into the reaction chamber. The dopant distribution of these VLS grown nanowires was naturally inhomogeneous. This was shown by the surface etching experiments in the later section. To further increase such radial dopant inhomogeneity within nanowires, δ-doped nanowires were also prepared to study the effect of dopant spatial inhomogeneity on the thermoelectric properties. Si nanowires were grown under the temperature of 550 °C by introducing only SiH_4 (19 sccm) for 30 min. Subsequently, the temperature was elevated to 750 °C, and B_2H_6 (5 sccm) was introduced into the chamber for 1 min to perform δ-doping. The representative scanning electron microscopy (SEM) and transmission electron microscopy (TEM) images of as-grown B-doped Si nanowires are shown in Figure 1a and b, respectively. The diameters of these nanowires ranged from 20 to 200 nm.

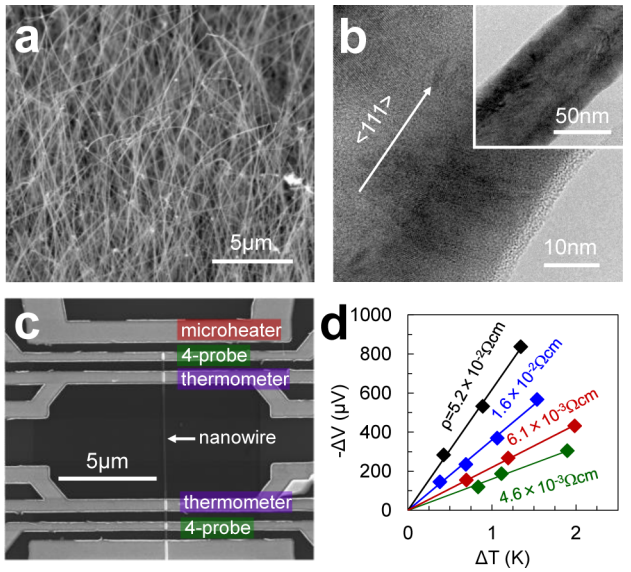

Figure 1. (a) SEM image of VLS grown B-doped Si nanowires, (b) TEM image of VLS grown B-doped Si nanowires, (c) SEM image of device configuration used in this work to characterize the resistivity and Seebeck coefficient, and (d) correlation data between thermovoltage ΔV and temperature difference ΔT to determine Seebeck coefficient S.

2.2. Seebeck Coefficient and Electrical Resistivity Measurement. The electrical measurements of Si nanowires were performed using 4-microprobe systems with the electrical characterization system (Keithley 4200SCS). Figure 1c shows the SEM image of device configuration fabricated by electron-beam lithography processes. All nanowire devices were fabricated on Si substrates with SiO_2 layer of 300 nm thickness. An external power source (WF1946, NF Co. Ltd.) was connected to the microheater in Figure 1c to generate the local temperature gradient. The thermovoltage ΔV and temperature difference ΔT along the Si nanowire were measured. Figure 1d shows typical results of the measured thermovoltage when varying the temperature difference ΔT. The linear relationship between the measured ΔV and ΔT was observed for the current temperature gradient range <2 K. The Seebeck coefficient $S = -\Delta V/\Delta T$ was then estimated from above linear relationship between ΔV and ΔT. Since an average temperature coefficient of resistivity (TCR) (~0.35%) of Pt thermometer was adopted during the determination of ΔT, the variation of TCR among different devices may lead to a statistical error of ~8% for the Seebeck coefficient. However, with the low noise level for ΔV measurement, the overall error for S determination was estimated to be <10%. The electrical resistivity of Si nanowires was determined from 4-probe measurements by using the formula: $\rho = R_{4\text{-probe}}\pi d^2/4L$, where $R_{4\text{-probe}}$, d, and L were the 4-probe resistance, nanowire diameter, and nanowire length, respectively. The nanowire diameter was estimated from the SEM and TEM images. See the details in Supporting Information sections 1−3. Note that the present Seebeck voltage measurements were reliably performed even for those highly resistive nanowires (the maximum resistance ~10^9 Ω) by utilizing a high input impedance (~10^{18} Ω) preamplifier equipped in the Keithley system. The raw thermovoltage measurement data for a relatively resistive nanowire (ρ = 100 Ωcm) is shown in Figure S1e.

2.3. Field Effect Measurements to Determine Hole Mobility and Carrier Concentration. The hole mobility was extracted from the field effect measurements by using the bottom Si substrate as the gate electrode. The gate voltage V_g was swept from −10 to 10 V, while the source-drain voltage V_{ds} was fixed to be 0.02 V. The hole mobility μ was determined from the measured transconductance curves (I_{ds} ~ V_g) using the formula, $\mu = (dI_{ds}/dV_g)L^2/(C_{gn}V_{ds})$, where L was the nanowire length and C_{gn} was the gate-nanowire coupling capacitance.[23] C_{gn} was approximated based on the "metal cylinder on plane" model,[24] in which it was expressed as $C_{gn} = 2\pi\varepsilon_0\varepsilon_r L/\cosh^{-1}(1/2 + d_{ox}/d)$, where ε_0, ε_r, and d_{ox} were the vacuum permittivity, dielectric constant, and thickness of the gate oxide, respectively. An effective value of ε_r = 2.2 was used for SiO_2 to address the dielectric discontinuity at the oxide−vacuum interface.[24] It is noted that, due to the metallic assumption, the approximation of C_{gn} was valid for heavily doped nanowires.[23] For lightly doped nanowires, the nanowire capacitance become small. As a result, the overall capacitance was strongly gate dependent, and nonlinear transconductance curve was observed. Thus, the hole mobility in this work was only extracted for those nanowires with ρ < 0.05 Ωcm, where the linear transconductance curve was observed. See details in the Supporting Information section 6.

2.4. Surface Etching on Si Nanowire Device. Surface etching of Si nanowire devices was performed by a wet etching process using the SC1 solution (NH_3H_2O:H_2O_2:H_2O = 1:1:5). In this solution, Si nanowires were fast oxidized by H_2O_2 and protected from overetching by the presence of NH_3H_2O. The overall etching rate was determined by the dissolution of SiO_2 in NH_3H_2O, which was ~1 nm/h for our conditions. After etching, the devices were thoroughly rinsed with water (80 °C) and isopropanol solvent to remove ions and organic residuals. The resulted surface density of states has been characterized to be as low as ~10^{12} cm^{-2},[25] which was almost similar to that of naturally oxidized H-terminated Si.

3. RESULTS AND DISCUSSION

First, we examine the thermoelectric properties of VLS grown B-doped Si nanowires. Figure 1a,b shows the SEM and TEM images of employed B-doped Si nanowires. The present Si nanowires were grown along the ⟨111⟩ growth direction.[26] The core−shell-like structures of present Si nanowires can be seen in the TEM images. This spatial inhomogenity has been considered as a consequence of VS film growth on the nanowire surface with the decomposition of dopant sources (B_2H_6).[20] As discussed by Amit et al., such a shell layer was dopant-rich when compared to the inner core, where the dopant atoms were merely incorporated into nanowires through metal catalyst.[20] Although we do not have the dopant distribution data, the existence of such heavily doped shell layer in the present B-doped Si nanowires is probed by a series of

dx.doi.org/10.1021/ja5055884 | J. Am. Chem. Soc. 2014, 136, 14100−14106

surface etching experiments, as will be discussed in the later section.

Figure 2a shows the measured Seebeck coefficient data for B-doped Si nanowires, whose electrical resistivity values were

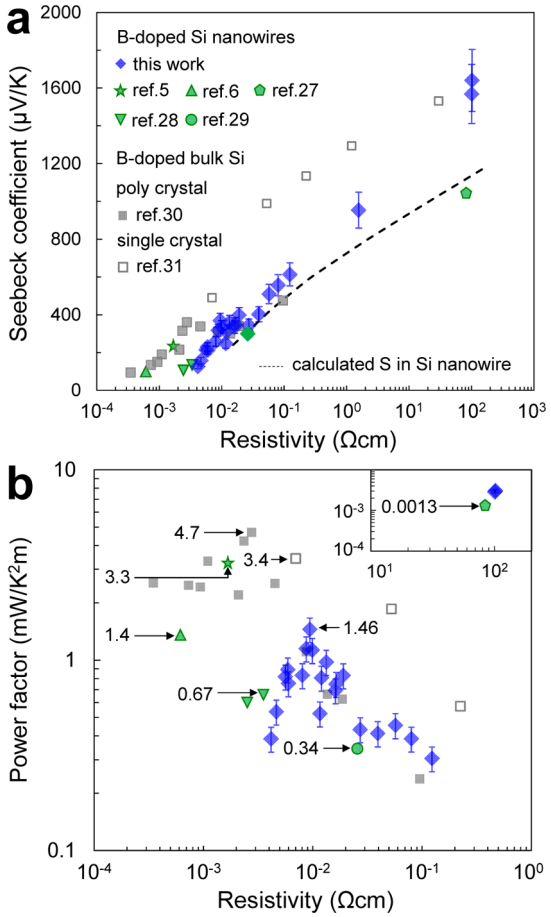

Figure 2. (a) Seebeck coefficient and (b) power factor data of present VLS grown B-doped Si nanowires as a function of resistivity. For comparison, reference data of homogeneously B-doped Si and the theoretical calculated line based on the Mott relation are shown.

ranged from 10^{-3} to 10^{2} Ωcm. Although the nanowires were collected from the same sample, the resistivity values were widely distributed. We found that the resistivity distribution of nanowire is mainly caused by the variation of apparent dopant concentrations within nanowires rather than surface damages during device fabrication process, as shown in the Supporting Information section 4. Note that we intentionally utilized the resistivity distribution to examine the correlation between the Seebeck coefficient and electrical resistivity. The reference data of Seebeck coefficients for B-doped Si nanowires,[5,6,27−29] polycrystalline[30] and single crystalline[31] samples are shown in Figure 2. Since the phonon-drag effects were negligible in nanowires, the present data of nanowires should be compared to the reference data for nanostructures and polycrystalline samples, where the electronic contribution on the Seebeck coefficient is dominant. As seen in Figure 2a, for a relatively low resistivity range below 10^{-2} Ω cm, both the nanowire and the reference values were ranged below 400 μV/K. Above 10^{-2} Ω cm, the Seebeck coefficient value of nanowires tends to be significantly higher than the reference data. For the resistivity ∼10^{2} Ω cm, the Seebeck coefficient value (∼1640 μV/K) was ∼1.6 times higher than the reference data (∼1000 μV/K). In such lightly doping region, the theory based on so-called Mott relation well describes the electric contribution of Seebeck coefficients,[32] as shown in Figure 2a (dashed line). The calculation was performed based on the nondegenerated assumption of Si by using the resistivity values estimated from the empirical hole mobility in B-doped Si.[33,34] Details of the calculation can be seen in the Supporting Information section 5. As can be seen, the theoretical prediction based on the Mott relation well predicted the Seebeck coefficient for homogeneously B-doped Si samples, but not for the present B-doped Si nanowires. Figure 2b shows the comparison between the present data and reference data on the power factor values. The power factor of present nanowires showed the maximum value (1.46 mW/K^2 m) at the resistivity of ∼10^{-2} Ω cm, which is still lower than the optimized power factor data (4.7 mW/K^2 m)[30] for homogeneously B-doped Si polycrystalline samples at the lower resistivity range of 3 × 10^{-3} Ω cm. The data of ref 5 for B-doped Si nanowires, which were treated by postgrowth gas-phase B doping (i.e., the possible spatial dopant inhomogeneity), showed the only higher power factor value (3.3 mW/K^2 m); however, other previous power factor values of homogeneously B-doped Si nanowires were lower than the maximum value of the present nanowires.

There are several possible scenarios to explain the observed modulation of power factor in the present B-doped Si nanowires. First, the Seebeck coefficient value can be increased by a low dimensional quantum effect on the density of states according to the theoretical predictions.[7] However, considering the present nanowire size range down to 20 nm, the temperature range employed (room temperature) and the Bohr radius required for quantization (∼4.3 nm), such a quantum effect is unlikely to emerge within the limit of the present experiments.[35] As indirect evidence, the electrical transport properties of the present Si nanowires did not show any apparent diameter dependences, as shown by Figure S3 in the Supporting Information. This result also excludes the role of surface states on the observed modulation of power factor. The other scenario is based on the presence of inhomogeneous dopant distribution within our B-doped Si nanowires grown by VLS process (i.e., heavily doped outer shell and lightly doped inner core). If there is a difference between the heavily doped outer shell and the lightly doped inner core on the electrical conductivity due to the different dopant concentration, the variation of physical properties should also exist along the radial direction of present nanowires.[36] Thus, the combination of both core and shell properties, including the Seebeck coefficient and conductivity, determines the physical properties of nanowires.[37] In addition, the mobile carriers might diffuse from the heavily doped outer shell to the lightly doped inner core to align the Fermi level, as can be seen in our calculation data in Supporting Information section 7. If such diffused carriers exist in the lightly doped core, the apparent mobility of nanowires should be increased when compared with homogeneously doped systems due to the suppression of ionized impurity scattering.

To examine the above scenario, the field effect measurements were performed to extract the mobility and the carrier concentration in our B-doped Si nanowires. Figure 3 shows the extracted hole mobility data plotted as a function of the hole carrier concentration. Reference data of homogeneously B-doped Si are shown for comparison.[33,38] As seen in the figure, the mobility data of the present B-doped Si nanowires were

dx.doi.org/10.1021/ja5055884 | J. Am. Chem. Soc. 2014, 136, 14100−14106

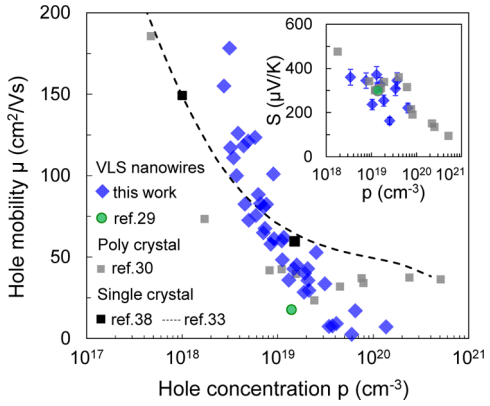

Figure 3. Hole mobility data of present VLS grown B-doped Si nanowires as a function of hole concentration, which were determined by field effect measurements. For comparison, the reference data for B-doped Si systems are shown in the figure. The inset shows the extracted relationship between Seebeck coefficient data and hole concentration.

higher than the data of homogeneously B-doped Si when the carrier concentration was ranged below around 10^{19} cm^{-3}. This carrier concentration range is in fact well consistent with the resistivity range $\rho > 10^{-2}$ Ω cm in Figure 2, where the Seebeck coefficient and the power factor tend to deviate from the reference data of homogeneously B-doped Si. When the carrier concentration was higher than 10^{19} cm^{-3}, the hole mobility was lower than those of the homogeneously B-doped system. Note that the lower mobility values were comparable with those of earlier VLS grown B-doped Si nanowires.[29] In such heavily B doping range for nanowires, the degraded crystallinity[39,40] due to the presence of nonactivated B dopants possibly lowers the hole mobility. From the hole mobility and electrical resistivity data, we examine the relation between the Seebeck coefficient and the carrier concentration, as shown in the inset of Figure 3. There was no significant difference between the present nanowires and homogeneously B-doped Si on the Seebeck coefficient data as a function of the carrier concentration. Thus, the mobility enhancement increases overall electrical conductivity of nanowires without reducing the Seebeck coefficient value, which increases the power factor of nanowires. Hence, these mobility data are consistent with the scenario based on the presence of inhomogeneous dopant radial distribution to explain the observed modulation of the power factor. Since the hole mobility of the nanowire tended to be lower than that of bulk Si due to the degraded crystallinity in the doping range above 10^{19} cm^{-3}, the applicability of the present method based on dopant modulation effects seems to be limited. One of the possible approaches to overcome this limitation might be the use of rapid thermal annealing[41] to enhance the crystallinity of nanowires.[42]

Here we question the inherent nature of mobility enhancement when the radial dopant profile exists. In general, the hole mobility depends on the effective hole mass and scattering mechanism. Since the effective hole mass in the ⟨111⟩ direction in Si is relatively heavy,[43] the modulation of mobility by the growth direction of nanowire is unlikely to occur. The other scenario is based on the difference between the inner core and the outer shell on the carrier scattering. If the sharp gradient of B dopant concentration exists in the radial direction of the present nanowires (heavily doped outer shell/lightly doped inner core), the carrier diffusion from the outer shell to the inner core might occur, as supported by our electrostatic simulations in Supporting Information section 7. This might enhance the apparent mobility of nanowires when compared with homogeneously doped nanowires due to the decreased impurity scattering in the inner core.

Next, we experimentally probe the existence of the heavily B-doped shell within Si nanowires by performing a wet etching of the Si nanowire surface. This is because the conventional composition analysis methods are not capable of detecting the low concentration of B dopants within the present Si nanowires.[17,22] The etching experiments were performed by using the widely used SC1 solution (H_2O_2:NH_3/H_2O:H_2O = 1:1:5) for Si processing.[25] Figure 4a shows the schematic of the

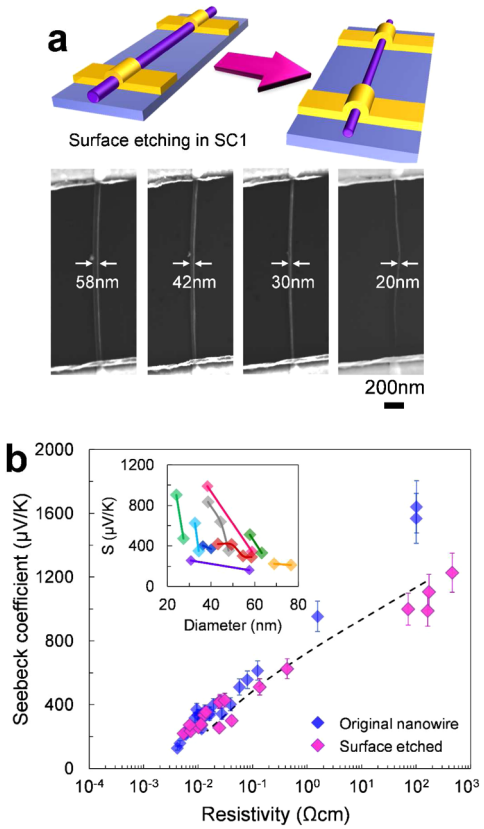

Figure 4. (a) Schematic illustration of the in situ surface etching process of Si nanowire device, and the representative SEM images of nanowire devices after surface etching treatments. (b) Effect of surface etching treatments on Seebeck coefficient data as a function of resistivity. The inset shows the variation of Seebeck coefficient data as a function of nanowire diameters during etching. Each color mark stands for the same nanowire device.

etching experiments. The nanowires were etched on the device. In the SC1 solution, the surface oxide on Si nanowire was slowly etched (~1 nm/h) by NH_3/H_2O, while H_2O_2 was used to protect the nanowire from overetching by fast reoxidizing the exposed Si surface. Figure 4a also shows the representative SEM images of the etched nanowires. The nanowire diameter was continuously reduced from 58 to 20 nm after three steps of etching. The typical measured properties of the etched nanowires, including the resistivity, Seebeck coefficient, and mobility, are shown in Table 1. The device morphology and the measured transconductance curves before and after etching are supplied in Supporting Information section 8. We found that

dx.doi.org/10.1021/ja5055884 | J. Am. Chem. Soc. 2014, 136, 14100−14106

Table 1. Comparison between the Original VLS Grown B-Doped Si Nanowires and Nanowires after Surface Etching on the Physical Properties Including Diameter, Resistivity, Seebeck Coefficient, Hole Mobility, and Carrier Concentration

sample	diameter (nm)	resistivity (Ω cm)	S (μV/K)	μ (cm^2/(V s))	p (cm^{-3})
original	63	9.94×10^{-3}	356	82.41	7.63×10^{18}
after etching	57	1.35×10^{-1}	511[a]	273.67	1.69×10^{17}

[a]Theoretical prediction: $p = 1.69 \times 10^{17}$ cm^{-3}, $S \sim 527$ μV/K.

removing slightly the surface layer (~3 nm) significantly increased the resistivity, Seebeck coefficient, and hole mobility. These variations are consistent with the presence of the heavily doped shell in the present B-doped Si nanowires. Especially, the observed enhancement of hole mobility cannot be explained by the surface etching damage effect, which in general decreases the carrier mobility. Thus, the enhanced mobility data in the etched nanowires supports the present scenario based on the inhomogeneous dopant profile (heavily doped shell and lightly doped inner core). In Figure 4b, we show the Seebeck coefficient data as a function of electrical resistivity for nanowire devices after surface etching treatments in comparison with the data of as-grown VLS grown nanowires and also the theoretical calculation data based on the Mott relation.[32,34] After surface etching, the Seebeck coefficient data of nanowires tend to be consistent with the theoretical prediction of the Mott relation, that is, the homogeneously B-doped Si. The inset shows the collected Seebeck coefficient variation on different nanowire devices, in which each mark stands for the same device. The Seebeck coefficient data increased with decreasing the nanowire diameter by etching. Since the Seebeck coefficient data should be constant if the homogeneous dopant distribution exists, the increased trend of Seebeck coefficient after etching also supports the presence of the heavily doped shell and lightly doped inner core in the present Si nanowires. Thus, these experimental results consistently support the critical role of the heavily doped outer shell on the observed modulation of power factor values.

Finally, we try to further enhance the role of heavily doped shell layer on the power factor. In principle, the thinner doped shell layer with sharper dopant gradient should enhance the contribution of diffused carriers from outer shell to inner core on the overall properties of nanowires. Thus, we create such thinner doped shell layer by utilizing surface δ-doping. The δ-doped nanowires were formed by preparing a heavily B-doped shell layer on the intrinsic Si nanowires, as illustrated by the inset of Figure 5a. Figure 5 shows the measured Seebeck coefficient and power factor data of δ-doped Si nanowires. For comparison, the data of B-doped Si nanowires grown by VLS process are shown in the figure. Interestingly, the Seebeck coefficient and power factor values of δ-doped nanowires were further increased and higher than those of VLS grown B-doped Si nanowires. This further enhancement of power factor values via δ-doping highlights the critical role of heavily doped shell layer thickness on the overall thermoelectric property of nanowires. Next, we examine the transport properties (mobility and carrier concentration) of δ-doped Si nanowires by performing field effect measurements to reveal the role of δ-doping on the power factor. The inset of Figure 5b shows the extracted hole mobility data of δ-doped nanowires as a function of the carrier concentration. In contrast to the transport data of Ge/Si core/shell nanowires with heterointerfaces,[15] the present δ-doped nanowires without heterointerfaces more steadily exhibited the mobility enhancement, possibly due to the absence of heterointerfaces. As shown in the figure, the mobility

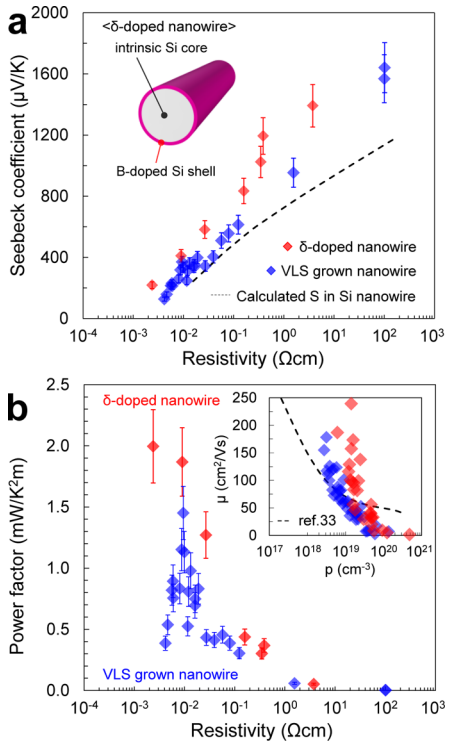

Figure 5. Comparison of (a) Seebeck coefficient and (b) power factor between the δ-doped Si nanowires and the VLS grown B-doped Si nanowires. The inset of (a) shows the schematic illustration of a δ-doped nanowire, composed by a intrinsic core and a heavily B-doped shell. The inset of (b) shows the comparison between measured hole mobility for δ-doped and VLS grown Si nanowires. The mobility enhancement was clearly consistent with the higher power factor for δ-doped nanowires.

values of δ-doped Si nanowires were statistically higher than those of VLS grown B-doped Si nanowires. Thus, this further mobility enhancement, which increases overall electrical conductivity without reducing Seebeck coefficient values, increases the power factor values of δ-doped nanowires. When compared to the data of bulk Si, the hole mobility of nanowires with dopant modulation tended to be lower in the doping range above 10^{19} cm^{-3}. As a result, the maximum power factor value in the present δ-doped Si nanowires is limited to 2.0 mW/K^2 m, which is lower than the optimized power factor value (4.7 mW/K^2 m) of polycrystalline samples[30] and the data of nanowires (3.3 mW/K^2 m) in a more heavily doped range.[5] When compared to the natural VLS grown Si nanowire, the superior properties of δ-doped Si nanowires clearly demonstrated the successful application of radial dopant modulation to engineer the thermoelectric performance of nanowires. As mentioned earlier, improving the dopant activation process (e.g., by rapid thermal annealing treatment[42]) in the present nanowires would be essential to further overcome the current limitation in enhancing the power factor over that of bulk materials. In the meantime, our present experimental results

dx.doi.org/10.1021/ja5055884 | J. Am. Chem. Soc. 2014, 136, 14100−14106

also infer that the thermoelectric power factor of Si nanowires can be further enhanced via more sophisticated dopant engineering in nanowires, that is, by creating thinner heavily doped shell layer on smaller diameter nanowires based on present δ-doped nanowires. Although we have shown the qualitative information as to the dopant spatial distribution, it would be an interesting issue to quantitatively correlate the real dopant spatial distribution of nanowires to thermoelectric properties by performing highly sensitive dopant profiling measurements (e.g., atom-probe tomography) or $C-V$ measurements.

4. CONCLUSION

In conclusion, we demonstrate the modulation of thermoelectric power factor via radially inhomogeneous dopant distributions in B-doped Si nanowires. The spatial distribution of B dopants within Si nanowires was inhomogeneous due to the sidewall vapor−solid growth during the vapor−liquid−solid nanowire growth, resulting in the heavily doped outer layer. The field effect measurements clarified that the hole mobility values of these nanowires were higher than those of homogeneously B-doped Si systems due to the dopant modulation effect. This mobility enhancement increases overall electrical conductivity of nanowires while without reducing the Seebeck coefficient value, resulting in the enhancement of thermoelectric power factor. In addition, we found that tailoring the surface dopant distribution by introducing δ-doping can further increase the power factor value. Thus, intentionally tailoring radial dopant inhomogeneity promises a way to improve the thermoelectric power factor of semiconductor nanowires with low thermal conductivity.

■ ASSOCIATED CONTENT

Supporting Information

Details of the Seebeck coefficient measurement, diameter calibration, error analysis, mobility extraction, a simulation of carrier diffusion under dopant gradient, additional detailed results from surface etching. This material is available free of charge via the Internet at http://pubs.acs.org.

■ AUTHOR INFORMATION

Corresponding Author

yanagi32@sanken.osaka-u.ac.jp

Notes

The authors declare no competing financial interest.

■ ACKNOWLEDGMENTS

This work was supported by NEXT Project. T.K. was supported by FIRST program. T.Y and K.U. are thankful for the financial support of CREST.

■ REFERENCES

(1) Snyder, G. J.; Toberer, E. S. *Nat. Mater.* **2008**, *7*, 105−114.
(2) Poudel, B.; Hao, Q.; Ma, Y.; Lan, Y. C.; Minnich, A.; Yu, B.; Yan, X. A.; Wang, D. Z.; Muto, A.; Vashaee, D.; Chen, X. Y.; Liu, J. M.; Dresselhaus, M. S.; Chen, G.; Ren, Z. F. *Science* **2008**, *320*, 634−638.
(3) Li, J. F.; Liu, W. S.; Zhao, L. D.; Zhou, M. *NPG Asia Mater.* **2010**, *2*, 152−158.
(4) Yang, J. H.; Yip, H. L.; Jen, A. K. Y. *Adv. Energy Mater.* **2013**, *3*, 549−565.
(5) Hochbaum, A. I.; Chen, R.; Delgado, R. D.; Liang, W.; Garnett, E. C.; Najarian, M.; Majumdar, A.; Yang, P. *Nature* **2008**, *451*, 163−167.
(6) Boukai, A. I.; Bunimovich, Y.; Tahir-Kheli, J.; Yu, J. K.; Goddard, W. A., 3rd; Heath, J. R. *Nature* **2008**, *451*, 168−171.
(7) Hicks, L. D.; Dresselhaus, M. S. *Phys. Rev. B* **1993**, *47*, 16631−16634.
(8) Tian, Y.; Sakr, M. R.; Kinder, J. M.; Liang, D.; MacDonald, M. J.; Qiu, R. L. J.; Gao, H.-J.; Gao, X. P. A. *Nano Lett.* **2012**, *12*, 6492−6497.
(9) Wu, P. M.; Gooth, J.; Zianni, X.; Svensson, S. F.; Gluschke, J. G.; Dick, K. A.; Thelander, C.; Nielsch, K.; Linke, H. *Nano Lett.* **2013**, *13*, 4080−4086.
(10) Dan, Y.; Seo, K.; Takei, K.; Meza, J. H.; Javey, A.; Crozier, K. B. *Nano Lett.* **2011**, *11*, 2527−2532.
(11) Ford, A. C.; Ho, J. C.; Chueh, Y. L.; Tseng, Y. C.; Fan, Z.; Guo, J.; Bokor, J.; Javey, A. *Nano Lett.* **2009**, *9*, 360−365.
(12) Lauhon, L. J.; Gudiksen, M. S.; Wang, C. L.; Lieber, C. M. *Nature* **2002**, *420*, 57−61.
(13) Xiang, J.; Lu, W.; Hu, Y. J.; Wu, Y.; Yan, H.; Lieber, C. M. *Nature* **2006**, *441*, 489−493.
(14) Zhao, Y. J.; Smith, J. T.; Appenzeller, J.; Yang, C. *Nano Lett.* **2011**, *11*, 1406−1411.
(15) Moon, J.; Kim, J.-H.; Chen, Z. C. Y.; Xiang, J.; Chen, R. *Nano Lett.* **2013**, *13*, 1196−1202.
(16) Martinez, J. A.; Cho, J.-H.; Liu, X.; Luk, T. S.; Huang, J.; Picraux, S. T.; Sullivan, J. P.; Swartzentruber, B. S. *Appl. Phys. Lett.* **2013**, *102*, 103101−5.
(17) Garnett, E. C.; Tseng, Y. C.; Khanal, D. R.; Wu, J.; Bokor, J.; Yang, P. *Nat. Nanotechnol.* **2009**, *4*, 311−314.
(18) Perea, D. E.; Hemesath, E. R.; Schwalbach, E. J.; Lensch-Falk, J. L.; Voorhees, P. W.; Lauhon, L. J. *Nat. Nanotechnol.* **2009**, *4*, 315−319.
(19) Fukata, N.; Ishida, S.; Yokono, S.; Takiguchi, R.; Chen, J.; Sekiguchi, T.; Murakami, K. *Nano Lett.* **2011**, *11*, 651−656.
(20) Amit, I.; Givan, U.; Connell, J. G.; Paul, D. F.; Hammond, J. S.; Lauhon, L. J.; Rosenwaks, Y. *Nano Lett.* **2013**, *13*, 2598−2604.
(21) Connell, J. G.; Yoon, K.; Perea, D. E.; Schwalbach, E. J.; Voorhees, P. W.; Lauhon, L. J. *Nano Lett.* **2013**, *13*, 199−206.
(22) Koren, E.; Berkovitch, N.; Rosenwaks, Y. *Nano Lett.* **2010**, *10*, 1163−1167.
(23) Khanal, D. R.; Wu, J. *Nano Lett.* **2007**, *7*, 2778−2783.
(24) Wunnicke, O. *Appl. Phys. Lett.* **2006**, *89*, 083102-3.
(25) Angermann, H.; Henrion, W.; Roseler, A.; Rebien, M. *Mater. Sci. Eng., B* **2000**, *73*, 178−183.
(26) Schmidt, V.; Senz, S.; Gosele, U. *Nano Lett.* **2005**, *5*, 931−935.
(27) Xu, B.; Li, C. B.; Thielemans, K.; Myronov, M.; Fobelets, K. *IEEE Trans. Electron Devices* **2012**, *59*, 3193−3198.
(28) Jang, M.; Park, Y.; Jun, M.; Hyun, Y.; Choi, S. J.; Zyung, T. *Nanoscale Res. Lett.* **2010**, *5*, 1654−1657.
(29) Brovman, Y. M.; Small, J. P.; Hu, Y. J.; Fang, Y.; Lieber, C. M.; Kim, P. 2013, arXiv:1307.0249v1. arXiv.org e-Print archive. http://arxiv.org/abs/1307.0249v1.
(30) Yamashita, O.; Sadatomi, N. *Jpn. J. Appl. Phys.* **1999**, *38*, 6394−6400.
(31) Geballe, T.; Hull, G. *Phys. Rev.* **1955**, *98*, 940−947.
(32) Krali, E.; Durrani, Z. A. K. *Appl. Phys. Lett.* **2013**, *102*, 143102-4.
(33) Masetti, G.; Severi, M.; Solmi, S. *IEEE Trans. Electron Devices* **1983**, *30*, 764−769.
(34) Ramayya, E. B.; Maurer, L. N.; Davoody, A. H.; Knezevic, I. *Phys. Rev. B* **2012**, *86*, 115328-11.
(35) Salleh, F.; Asai, K.; Ishida, A.; Ikeda, H. *Appl. Phys. Express* **2009**, *2*, 071203-3.
(36) Dillen, D. C.; Kim, K.; Liu, E. S.; Tutuc, E. *Nat. Nanotechnol.* **2014**, *9*, 116−120.
(37) Schlitz, R. A.; Perea, D. E.; Lensch-Falk, J. L.; Hemesath, E. R.; Lauhon, L. J. *Appl. Phys. Lett.* **2009**, *95*, 162101-3.
(38) Morin, F. J.; Maita, J. P. *Phys. Rev.* **1954**, *96*, 28−35.
(39) Lin, H. C.; Lin, H. Y.; Chang, C. Y.; Lei, T. F.; Wang, P. J.; Deng, R. C.; Lin, J. D.; Chao, C. Y. *Appl. Phys. Lett.* **1993**, *63*, 1525−1527.

(40) Fukata, N.; Mitome, M.; Sekiguchi, T.; Bando, Y.; Kirkham, M.; Hong, J.-I.; Wang, Z. L.; Snydert, R. L. *ACS Nano* **2012**, *6*, 8887−8895.
(41) Jeanjean, P.; Sellitto, P.; Sicart, J.; Robert, J. L.; Chaussemy, G.; Laugier, A. *Semicond. Sci. Technol.* **1991**, *6*, 1130−1134.
(42) Colli, A.; Fasoli, A.; Ronning, C.; Pisana, S.; Piscanec, S.; Ferrari, A. C. *Nano Lett.* **2008**, *8*, 2188−2193.
(43) Donetti, L.; Gamiz, F.; Thomas, S.; Whall, T. E.; Leadley, D. R.; Hellstrom, P. E.; Malm, G.; Ostling, M. *J. Appl. Phys.* **2011**, *110*, 063711-1.